J Mater Sci (2019) 54:12392–12400

Ceramics

Effects of phase composition and grain size on the piezoelectric properties of HfO_2-doped barium titanate ceramics

Hong-Mei Yin[1,2], Wen-Jun Xu[2], Heng-Wei Zhou[2], Xing-Yu Zhao[1,2], and Yi-Neng Huang[1,2,*]

[1] National Laboratory of Solid State Microstructures, School of Physics, Nanjing University, Nanjing 210000, People's Republic of China

[2] Xinjiang Laboratory of Phase Transitions and Microstructures in Condensed Matters, College of Physical Science and Technology, Yili Normal University, Yining 835000, People's Republic of China

Received: 13 March 2019
Accepted: 27 May 2019
Published online: 5 July 2019

ABSTRACT

The effect of grain size and phase compositions on piezoelectric coefficient of $BaTi_{0.98}Hf_{0.02}O_3$ ceramics prepared at a series of sintering temperatures (1320, 1350, 1370, and 1400 °C) was studied. The results showed that the grain size of the ceramics is 0.9, 21.3, 21.6, and 37.2 μm, respectively, and the corresponding phase compositions are the tetragonal–orthogonal, tetragonal–orthogonal–rhombohedral, tetragonal–orthogonal, and tetragonal–orthogonal–rhombohedral, while the piezoelectric coefficient is 475, 352, 258, and 327 pC/N, i.e., it decreases first and then increases as the grain size goes up. The phase compositions and grain size of the ceramics are interrelated, and they co-affect the piezoelectric coefficient.

Introduction

Developing the new materials with high piezoelectric coefficient (d_{33}) is one of the important fields of materials science. At present, the high d_{33} at room temperature mainly exists in $PbTiO_3$-based perovskite-type ferroelectrics, and they are widely used in pressure sensors, actuators, and ultrasonic imaging, etc. [1–3]. However, considering the Pb-based materials are harmful to human and environment, the exploration of lead-free piezoelectrics is one of the research priorities in this field [4–7].

Nearly 20 years, the lead-free ceramics with high d_{33} is developing rapidly. Based on compositions, it can be divided into three systems, such as $K_{1-x}Na_x$-NbO_3, $Bi_{1/2}Na_{1/2}TiO_3$ and $BaTiO_3$ (BT)-based ceramics [8]. BT ceramic is the earliest discovered piezoelectrics whose d_{33} is about 190 pC/N [1, 9]. At present, the higher d_{33} of 700 ± 30 pC/N at room temperature has been achieved in $0.82Ba(Ti_{0.89}$-$Sn_{0.11})O_3$–$0.18(Ba_{0.7}Ca_{0.3})TiO_3$ ceramic [10].

The mechanism of high d_{33} for BT-based ceramics is mainly studied as follows: (1) Relationship between high d_{33} and multiphase coexistence in a

Address correspondence to E-mail: ynhuang@nju.edu.cn

https://doi.org/10.1007/s10853-019-03726-y

specific system such as Ren et al. [11] reported the d_{33} of $BaZr_{0.2}Ti_{0.8}O_3$–$0.5Ba_{0.7}Ca_{0.3}TiO_3$ ceramic is 620 pC/N, which originates from the coexistence of rhombohedral (R) and tetragonal (T) phases due to the compositions being near the morphotropic phase boundary (MPB). Das et al. [12] found that $0.5BaZr_{0.2}Ti_{0.8}O_3$–$0.5Ba_{0.7}Ca_{0.3}TiO_3$–0.8 wt%CeO_2 ceramic has high d_{33} value (673 pC/N), while the R–T phases also coexist [13–17]. In a word, the multiphase coexistence in specific ceramic around MPB is favorable to the improvement in d_{33}, but the effect of the phase ratios on d_{33} is not clear; and (2) relationship between high d_{33} and grain size (g) in a specific system. For example, with decreasing g, d_{33} increases in BT ceramics found by Hoshina et al. [18], but reduces in the $Ba_{0.90}Ca_{0.10}Ti_{0.90}Sn_{0.10}O_3$–$xY_2O_3$ one, and it increases first and then decreases in $Ba_{1-x}Ca_xTi_{0.90}Sn_{0.10}O_3$–$0.08Dy_2O_3$ obtained by Chen et al. [19–21].

In addition, the domain structures also have some influence on the d_{33}. For instance, Li et al. [22] have reported "blurred" grain boundaries may reduce the internal stress and lead to the formation of continuity of domains across the boundaries, resulting in the d_{33} of $BaZr_{0.2}Ti_{0.8}O_3$–$0.5Ba_{0.7}Ca_{0.3}TiO_3$ ceramic up to 650 pC/N. Besides, Das et al. [23] studied the domain widths of some $BaZr_{0.2}Ti_{0.8}O_3$–$0.5Ba_{0.7}Ca_{0.3}TiO_3$ ceramics with larger d_{33} and found that the largest d_{33} corresponds to the widest 90° domains. Li et al. [24] found $0.5BaZr_{0.2}Ti_{0.8}O_3$–$0.5Ba_{0.7}Ca_{0.3}TiO_3$–xZnO can achieve the highest domain wall density at $x = 0.08$, at the same time, d_{33} (603 pC/N) is the maximum.

$BaTi_{1-x}Hf_xO_3$ and $BaTi_{1-x}Zr_xO_3$ ceramics have similar phase diagrams [25–27] and piezoelectric properties [9, 28, 29]. However, there is still no $BaTi_{1-x}Hf_xO_3$-based ceramic whose d_{33} exceeds 600 pC/N [28–38]. Therefore, it is necessary to analyze and study the influence factors to d_{33} in $BaTi_{1-x}Hf_xO_3$ ceramics. Up to now, as far as the authors know, there is no study on the co-effect of multiphase coexistence and g on the high d_{33} in a specific system. Moreover, it has been found that $BaTi_{1-x}Hf_xO_3$ ceramics may be MPB near $x = 0.04$ [25, 31], and could have larger d_{33}. In this paper, $BaTi_{0.98}Hf_{0.02}O_3$ (BTH) ceramics were selected as a candidate system and prepared by solid-state reaction at a series of sintering temperatures (T_s). The influence of phase compositions and g on d_{33} was studied by measuring and analyzing the room temperature d_{33}, hysteresis loop, phase compositions, g, and temperature-dependent complex dielectric constant of the ceramics.

Experimental procedure

BTH ceramics were prepared by the conventional solid-state reaction technique with various T_s. High purity (99.99%) powders of $BaCO_3$, TiO_2, and HfO_2 were used as starting materials. The ingredients were weighed in stoichiometric proportions and wet-mixed with deionized water. After 16 h mixing and then drying, the powder was calcined at 1100 °C for 2 h in air, and $BaCO_3$, TiO_2, and HfO_2 reacted to form BTH powders. The powders with 2.5 wt% binders were compacted into disk-shaped pellets with a diameter of 13.0 mm and thickness of 1.0–2.0 mm at 10 MPa pressure, followed by burning the binder. BTH pallets were sintered at $T_s = 1320$, 1350, 1370, and 1400 °C for 4 h in air.

The room temperature phase compositions and g of BTH ceramics were tested by DX-2600 X-ray diffractometer and KYKY2800B scanning electron microscope (SEM).

The sintered specimens were coated with silver paint on the upper and bottom surfaces and fired at 850 °C for 15 min for electrical measurements. The room temperature hysteresis loops of specimens were performed using the TF Analyzer 2000E at 1 Hz, and the coercive field (E_c) and remnant polarization (P_r) were obtained. The poling process was performed under a static electric field of $2.5E_c$ at room temperature for 20 min in a silicone oil bath, and after 24 h, d_{33} was measured by Piezotest PM300 at room temperature, 300 Hz, and 0.5 N. The complex dielectric constant ($\varepsilon^* = \varepsilon' - i\varepsilon''$) of the specimens was carried out in the temperature range of 100–430 K with heating rate 2 K/min and frequency range of 100 Hz–10 kHz.

Results and discussion

Figure 1a shows d_{33} of BTH ceramics at room temperature sintered at various T_s. It can be seen that the overall trend of d_{33} reduces with increasing T_s, and specifically, d_{33} are 475, 327, 352, and 258 pC/N corresponding to $T_s = 1320$, 1350, 1370, and 1400 °C. The hysteresis loops at room temperature of BTH

ceramics are given in Fig. 1b. All ceramics exhibit the ferroelectric behaviors, which suggest that they are in the ferroelectric phase at room temperature, and the results agree precisely with the characteristic of $BaTi_{1-x}Hf_xO_3$ phase diagram [25]. $2E_c$ and $2P_r$ are read from Fig. 1b and plotted in Fig. 1c, d. The variation trend of $2E_c$ is the same as that of d_{33}, but $2P_r$ decreases at first and then increases.

Figure 2 illustrates SEM images (Fig. 2a–d) and the corresponding statistical distribution of grain size (Fig. 2e–h) of BTH ceramics for various T_s, we can find that g are 0.9, 37.2, 21.3, and 21.6 μm for $T_s = 1320$, 1350, 1370, and 1400 °C as shown in Fig. 1e. Compared with 1320 °C, the samples sintered at other T_s have wide distribution of g. Obviously, the variation trend of g is opposite to that of d_{33}, but it is not inverse linear by comparing Fig. 1a, e, and it is different from that of pure BT ceramics [18, 39]. d_{33} is maximum when g = 0.9 μm, which is larger than the reported values of $BaTi_{1-x}Hf_xO_3$ [28, 38], $BaTi_{1-x}Zr_xO_3$ [40, 41], $BaTi_{1-x}Sn_xO_3$ [42] ceramics at room temperature, but similar to that value obtained by two-step sintering methods [18, 43]. Because the fine-grained ceramics have a high density of 90° domain walls that is easily moved by an external ac field, high d_{33} can be obtained [18, 43–45].

The room temperature X-ray diffraction patterns of BTH ceramics sintered at series T_s are shown in Fig. 3, and the results indicate that all samples have a pure perovskite phase without visible impurity phase (Fig. 3a). The detailed structural characterization of peaks around 39°, 45°, and 65° is also carried out in Fig. 3b–d.

The standard XRD spectra of BT show that: (1) Cubic (C) phase: Single diffraction peaks appear near 39°, 45°, and 65°, corresponding to (111), (200), and (220) planes, respectively; (2) T phase: Single peak appear near 39°, double peaks of left low and right high near 45°, and double peaks of left high and right low near 65°; (3) O phase: Single peak appear near 39°, double peaks of right low and left high near 45°, and triple peaks near 65°; and (4) R phase: Double peaks appear near 39°, single peak near 45°, and double peaks of right high and left low near 65°. By the standard spectrum of BT and the method in Refs. [13, 16], the fitting results of diffraction peaks near 39°, 45° and 65° of BTH ceramics (Fig. 3b–d) show that the T–O phases coexist in ceramics for $T_s = 1400$ °C and 1320 °C, while T–O–R phases for $T_s = 1370$ °C and 1320 °C. We would like to point out that, compared with $T_s = 1320$ °C, the overall high-angle peak shift of the sample for $T_s = 1400$ °C means the cell volume being smaller (Fig. 3a). One possible origination is the different surface effects of grains with different g, and another is the different proportions of T and O phases in the ceramics at different T_s.

Combining with the corresponding values of d_{33} and g, it is found that the smaller g correspond to higher d_{33} when ceramics have the same phase

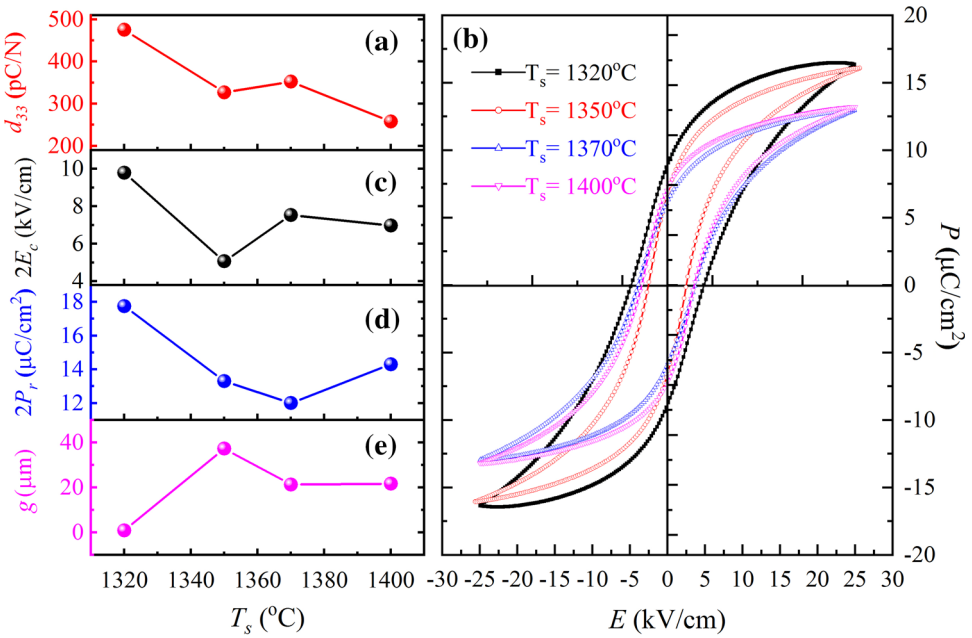

Figure 1 d_{33} (**a**), hysteresis loops (**b**), $2E_c$ (**c**), $2P_r$ (**d**), and g (**e**) of BTH ceramics at room temperature for various T_s.

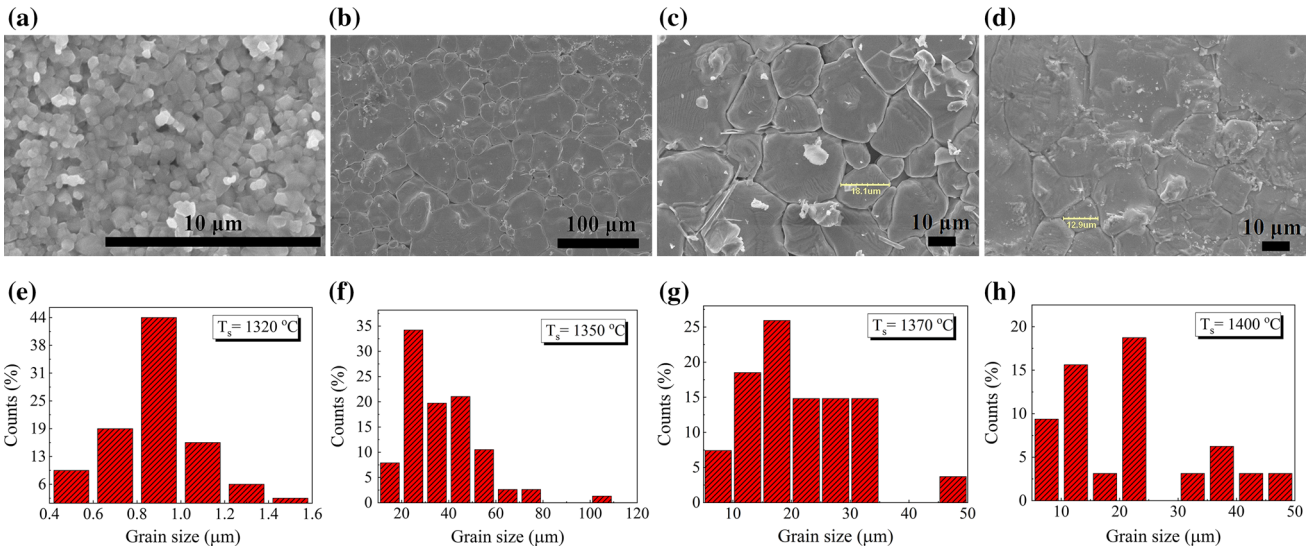

Figure 2 SEM images of BTH ceramics: **a** T_s = 1320 °C, **b** T_s = 1350 °C, **c** T_s = 1370 °C, **d** T_s = 1400 °C. **e**–**h** The corresponding grain size distributions.

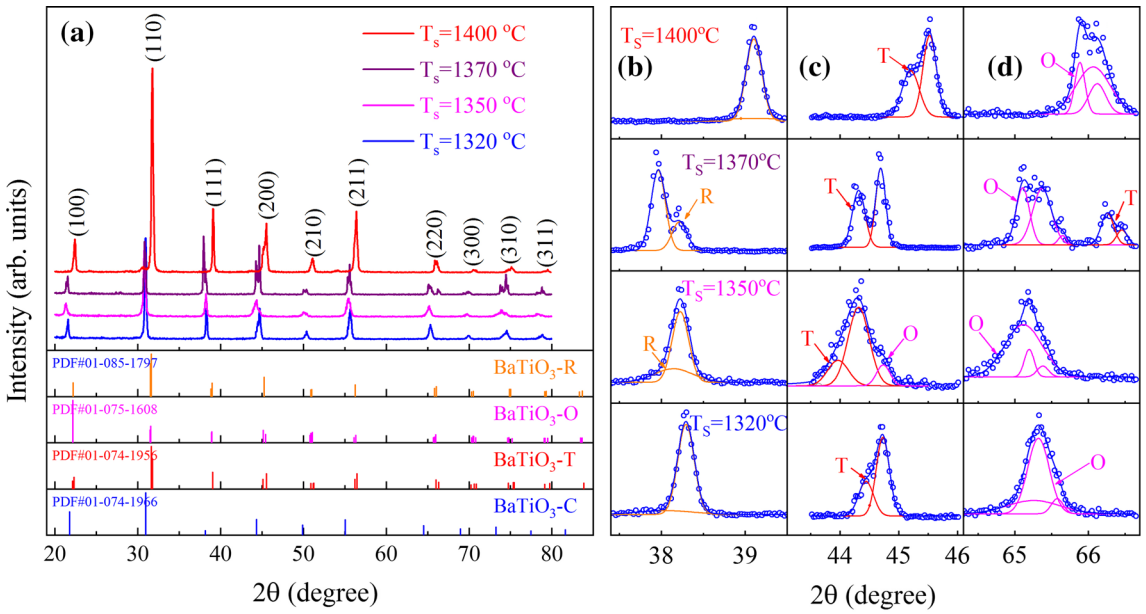

Figure 3 Room temperature XRD patterns of BTH ceramics sintered at various T_s. 2θ values are **a** 20°–80°; **b** 37°–40°; **c** 43.1°–46.1°; **d** 64.3°–66.7°. In **b**–**d** experimental results, accumulation peaks, fitted peaks of T phase, fitted peaks of O phase, fitted peaks of R phase.

compositions. Therefore, it is necessary to consider the effect of phase compositions when discussing the relationship between d_{33} and g.

Figure 4 illustrates ε' and ε'' of ε^* for BTH ceramics measures at various frequencies and temperatures (T). The results indicate that, similar to pure [46, 47] and low Hf-doped $BaTiO_3$ ceramics [25, 28, 48, 49], there are three phase transitions, i.e., C–T, T–O, and O–R, in 100–430 K, and the corresponding transition temperatures (T_C, T_{TO}, and T_{OR}) vary with T_s. According to the variation of ε' and ε'' versus T, it could be seen that the T–O phase transition is diffuse and broad, which may be caused by the uneven distribution of Hf, g distribution, and influence of grain boundaries. It leads to T–O phase coexistence near room temperature. Accordingly, the characteristic peaks of T and O phase were found in XRD spectra of BTH ceramics (Fig. 3c, d).

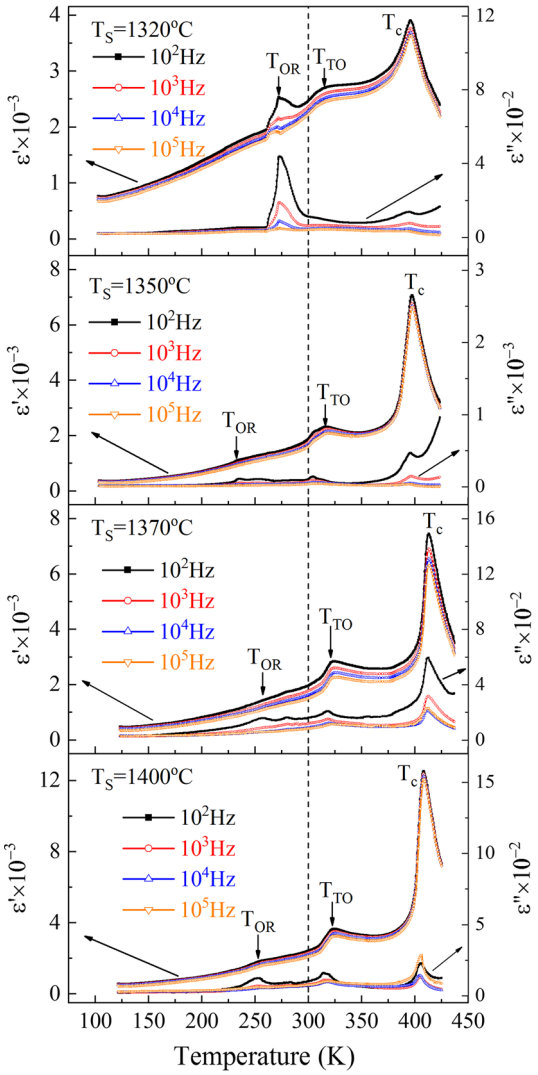

Figure 4 Temperature dependence of ε' and ε'' for BTH ceramics with various T_s.

Based on the peak heights of ε' and ε'', the amount of transition between R and O phases and the room temperature content of O phase in the BTH ceramic for $T_s = 1320$ °C are larger than the other, and it is one reason for the larger d_{33} of the ceramic because O phase can bring about exceptionally low elastic modulus [50]. When $T_s = 1350$ °C and 1370 °C, the relative variation of ε'' from T_{TO} to T_{OR} is small, and it can be inferred that O–R phase transition diffuses to higher temperatures due to possible random internal stress, which causes a few amount of R phase to exist when the temperature is much higher than T_{OR}. Therefore, the characteristic peaks of R phase can be found in the XRD spectra (Fig. 3b). While $T_s = 1400$ °C, there is no characteristic peaks of R phase in the XRD spectra (Fig. 3b) due to the smaller dispersion of O–R phase transition.

As shown in Fig. 5a, with increasing T_s, (1) T_C goes up first and then down; (2) T_{TO} always increases; and (3) T_{OR} decreases first, then goes up and finally down, while, with increasing g, (4) both T_C and T_{TO} first go up and then down; and (5) T_{OR} always decreases (Fig. 5b). In which, the increase in T_C with g for $g \leq 21.3$ μm could be explained by the grain size effect [51]; however, the decrease in T_C for $g \geq 21.3$ μm must contain other influencing factors, such as oxygen vacancies [52] and internal stress [51]. For the T–O and O–R phase transitions related to the coupling between the spontaneous polarizations and spontaneous strains, the influence of g, oxygen vacancies and internal stress to the coupling is not quite clear now.

The room temperature ε' at 100 Hz with g and phase compositions for BTH ceramics of series T_s is shown in Fig. 6a, and it could be seen that, (1) for the ceramics of the same phase compositions, the smaller the g is, the larger the ε' is; and (2) the ε' of the ceramics of T–O phases is larger than that of the T–O–R ones. One possible corresponding mechanism is that, (1) the samples of T–O phases may contain more T phase than those of T–O–R phases, and T phase has higher density of 90° domain walls, which leads to the increase in ε' [53, 54]; and (2) when the phase compositions are the same, the smaller the g is, the higher the domain wall density of 90° domains is [54].

Figure 1d shows that, with T_s, the change trend of P_r is contrary to that of cell volume (Fig. 3), and the cell volume is related to phase compositions and g. As indicated by Fig. 6b, although the values of g (21.3 μm for $T_s = 1370$ °C) and (21.6 μm for $T_s = 1400$ °C) are almost same, P_r of the ceramics with T–O phases is larger than that of T–O–R ones, i.e., P_r is different because of the different phase compositions. Moreover, when the ceramics have same phase compositions, P_r are also different with different g. Figure 6c clearly indicates that E_c decreases with the increase in g, which may be caused by the decrease in internal stress with the decrease in g [54, 55].

According to the above analyses, the variation of d_{33} for BTH ceramics with g and phase compositions are shown in Fig. 6d. It is found that, with increasing g, d_{33} decreases first and then increases, and when the

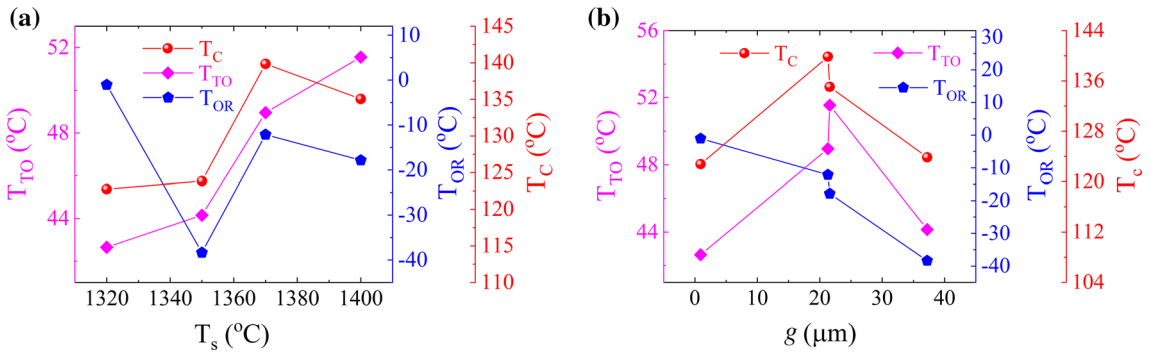

Figure 5 T_C, T_{TO}, and T_{OR} for BTH ceramics with various **a** T_s and **b** g at 100 Hz.

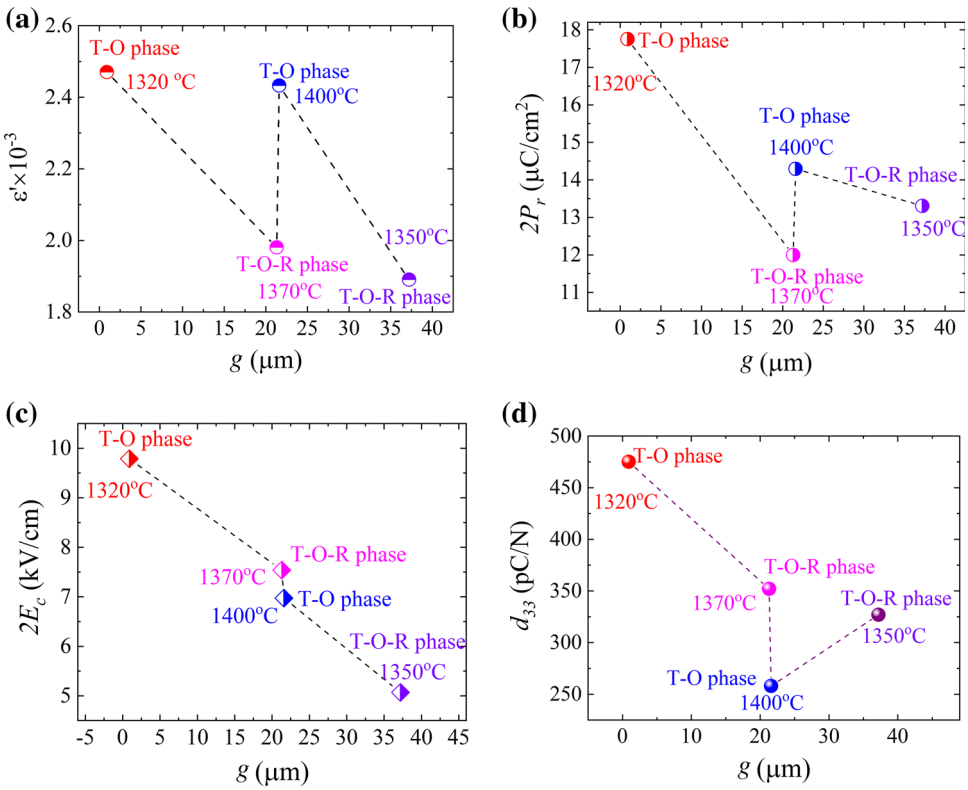

Figure 6 Room temperature ε' (**a**), P_r (**b**), E_c (**c**), and d_{33} (**d**) versus g and phase compositions for BTH ceramics of series T_s.

ceramics have the same phase compositions, the larger the g is, the smaller the d_{33} is. Specifically, for $g = 0.9$, 21.3, 21.6, and 37.2 μm, the phase compositions of the ceramics are T–O, T–O–R, T–O, and T–O–R phases, respectively, and d_{33} decreases with increasing g, which indicates d_{33} is mainly affected by g when $g \leq 21.6$ μm [18, 39]. However, d_{33} goes up when $g \geq 21.6$ μm, i.e., d_{33} of T–O–R phase coexistence is higher than that of T–O, so it is mainly affected by phase compositions, which is consistent with the conclusion that the multiphase coexistence of T–O–R leads to a low energy barrier for the polarization rotations, resulting in the high d_{33} [16, 42, 56, 57].

The author considers that the reasons for the increase in d_{33} with the decrease in g in ceramics of same phase compositions are as follows: (1) With the decrease in g, the ratio of surface layer to volume of the grains increases; and (2) the interaction energy between a permanent dipole and its neighbors in the surface layer is higher than that of the permanent dipole in grain interior, i.e., its stability is lower. In other words, under the same external stress, the dipoles in the surface layer are more likely to be

oriented and polarized, resulting in higher piezoelectric coefficients.

It is worthwhile pointing out that the Ranjan et al. [28] reported d_{33} of BTH ceramic of O–T phases (sintered 1300 °C for 4 h and then 1450–1500 °C for 6 h) is 370 pC/N, much smaller than 475 pC/N in this work. It can be expected that g of the ceramic of Ranjan et al. is much larger than ours (sintered at 1320 °C for 4 h), which is consistent with the results of Fig. 6d in this paper.

Conclusions

BTH ceramics near MPB were prepared by traditional solid-state reaction at series T_s. The room temperature d_{33}, $2P_r$, $2E_c$, g, and phase compositions, as well as ε' and ε'' with temperature at series frequencies were tested and analyzed. The results indicate that, when $T_s = 1320$, 1350, 1370, and 1400 °C, d_{33} is 475, 327, 352, and 258 pC/N, g is 0.9, 37.2, 21.3, and 21.6 μm, and the corresponding phase compositions are T–O, T–O–R, T–O–R, and T–O phases, respectively. In other words, with increasing g, d_{33} decreases first and then increases, and when the ceramics have the same phase compositions, the larger the g is, the smaller the d_{33} is. Therefore, the phase compositions and g of the ceramics are interrelated and co-affect d_{33}.

Acknowledgements

This work is supported by the Natural Science Foundation of China (Grant No. 11664042).

Compliance with ethical standards

Conflict of interest The authors declare that they have no conflicts of interest to this work.

References

[1] Jaffe H, Berlincourt DA (1965) Piezoelectric transducer materials. Proc IEEE 53(10):1372–1386. https://doi.org/10.1109/PROC.1965.4253

[2] Cross E (2004) Materials science: lead-free at last. Nature 432(7013):24–25. https://doi.org/10.1038/nature03142

[3] Zhang SJ, Li F, Yu FP, Jiang XN, Lee HY, Luo J, Shrout TR (2018) Recent developments in piezoelectric crystals. J Korean Ceram Soc 55(5):419–439. https://doi.org/10.4191/kcers.2018.55.5.12

[4] Rödel J, Webber KG, Dittmer R, Jo W, Kimura M, Damjanovic D (2015) Transferring lead-free piezoelectric ceramics into application. J Eur Ceram Soc 35(6):1659–1681. https://doi.org/10.1016/j.jeurceramsoc.2014.12.013

[5] Wu JG, Xiao DQ, Zhu JG (2015) Potassium–sodium niobate lead-free piezoelectric materials: past, present, and future of phase boundaries. Chem Rev 115(7):2559–2595. https://doi.org/10.1021/cr5006809

[6] Shrout TR, Zhang SJ (2007) Lead-free piezoelectric ceramics: alternatives for PZT? J Electroceram 19(1):113–126. https://doi.org/10.1007/s10832-007-9047-0

[7] Wang XP, Wu JG, Xiao DQ, Zhu JG, Cheng X, Zheng T, Zhang BY, Lou XJ, Wang XJ (2014) Giant piezoelectricity in potassium–sodium niobate lead-free ceramics. J Am Chem Soc 136(7):2905–2910. https://doi.org/10.1021/ja500076h

[8] Trolier-McKinstry S, Zhang SJ, Bell AJ, Tan XL (2018) High-Performance piezoelectric crystals, ceramics, and films. Annu Rev Mater Res 48:191–217. https://doi.org/10.1146/annurev-matsci-070616-124023

[9] Acosta M, Novak N, Rojas V, Patel S, Vaish R, Koruza J, Rossetti GA, Rödel J (2017) $BaTiO_3$-based piezoelectrics: fundamentals, current status, and perspectives. Appl Phys Rev 4(4):41305. https://doi.org/10.1063/1.4990046

[10] Zhao CL, Wu HJ, Li F, Cai YQ, Zhang Y, Song DS, Wu JG, Lyu X, Yin J, Xiao DQ, Zhu JG, Pennycook SJ (2018) Practical high piezoelectricity in barium titanate ceramics utilizing multiphase convergence with broad structural flexibility. J Am Chem Soc 140(45):15252–15260. https://doi.org/10.1021/jacs.8b07844

[11] Liu WF, Ren XB (2009) Large piezoelectric effect in Pb-free ceramics. Phys Rev Lett 103(25):257602. https://doi.org/10.1103/PhysRevLett.03.257602

[12] Chandrakala E, Paul Praveen J, Kumar A, James AR, Das D, Damjanovic D (2016) Strain-induced structural phase transition and its effect on piezoelectric properties of (BZT-BCT)-(CeO_2) ceramics. J Am Ceram Soc 99(11):3659–3669. https://doi.org/10.1111/jace.14409

[13] Zhou PF, Zhang BP, Zhao L, Zhao XK, Zhu LF, Cheng LQ, Li JF (2013) High piezoelectricity due to multiphase coexistence in low-temperature sintered (Ba, Ca)(Ti, Sn)O_3-CuOx ceramics. Appl Phys Lett 103(17):172904. https://doi.org/10.1063/1.4826933

[14] Long PQ, Liu XT, Long X, Yi ZG (2017) Dielectric relaxation, impedance spectra, piezoelectric properties of (Ba, Ca)(Ti, Sn)O_3 ceramics and their multilayer piezoelectric actuators. J Alloys Compd 706:234–243. https://doi.org/10.1016/j.jallcom.2017.02.237

[15] Jiang XP, Li L, Chen C, Tang J, Zheng KP, Li XH (2014) Structure and properties of $(Ba_{0.85}Ca_{0.15})(Ti_{0.9}Zr_{0.1-x}Sn_x)O_3$ lead-free ceramics with high piezoelectric constant. J Inorg Mater 29(1):33–37. https://doi.org/10.3724/sp.J.1077.2014.13213

[16] Zhu LF, Zhang BP, Zhao XK, Zhao L, Yao FZ, Han X, Zhou PF, Li JF (2013) Phase transition and high piezoelectricity in (Ba, Ca)$(Ti_{1-x}Sn_x)O_3$ lead-free ceramics. Appl Phys Lett 103(7):72905. https://doi.org/10.1063/1.4818732

[17] Wu JG, Xiao DQ, Wu WJ, Chen Q, Zhu JG, Yang ZC, Wang J (2012) Composition and poling condition-induced electrical behavior of $(Ba_{0.85}Ca_{0.15})(Ti_{1-x}Zr_x)O_3$ lead-free piezoelectric ceramics. J Eur Ceram Soc 32(4):891–898. https://doi.org/10.1016/j.jeurceramsoc.2011.11.003

[18] Hoshina T, Hatta S, Takeda H, Tsurumi T (2018) Grain size effect on piezoelectric properties of $BaTiO_3$ ceramics. Jpn J Appl Phys 57(9):0902BB. https://doi.org/10.7567/jjap.57.0902bb

[19] Chen ZH, Li ZW, Qiu JH, Zhao TX, Ding JN, Jia XG, Zhu WQ, Xu JJ (2018) Y_2O_3 doped $Ba_{09}Ca_{0.1}Ti_{0.9}Sn_{0.1}O_3$ ceramics with improved piezoelectric properties. J Eur Ceram Soc 38(4):1349–1355. https://doi.org/10.1016/j.jeurceramsoc.2017

[20] Chen ZH, Li ZW, Ma MG, Qiu JH, Zhao TX, Ding JN, Jia XG, Zhu KQ (2018) Enhanced piezoelectric properties in $(Ba_{1-x}Ca_x)(Ti_{0.90}Sn_{0.10})O_3-0.08Dy_2O_3$ lead-free ceramics. Mater Res Bull 105:330–333. https://doi.org/10.1016/j.materresbull.2018.05.004

[21] Wu JG, Xiao DQ, Wu WJ, Chen Q, Zhu JG, Yang ZC, Wang J (2011) Role of room-temperature phase transition in the electrical properties of (Ba, Ca)(Ti, Zr)O_3 ceramics. Scr Mater 65(9):771–774. https://doi.org/10.1016/j.scriptamat.2011.07.028

[22] Wang P, Li YX, Lu YQ (2011) Enhanced piezoelectric properties of $(Ba_{0.85}Ca_{0.15})(Ti_{0.9}Zr_{0.1})O_3$ lead-free ceramics by optimizing calcination and sintering temperature. J Eur Ceram Soc 31(11):2005–2012. https://doi.org/10.1016/j.jeurceramsoc.2011.04.023

[23] Chandrakala E, Paul Praveen J, Hazra BK, Das D (2016) Effect of sintering temperature on structural, dielectric, piezoelectric and ferroelectric properties of sol-gel derived BZT-BCT ceramics. Ceram Int 42(4):4964–4977. https://doi.org/10.1016/j.ceramint.2015.12.009

[24] Zhao ZH, Li XL, Ji HM, Dai YJ, Li T (2015) Microstructure and electrical properties in Zn-doped $Ba_{0.85}Ca_{0.15}Ti_{0.90-}Zr_{0.10}O_3$ piezoelectric ceramics. J Alloys Compd 637:291–296. https://doi.org/10.1016/j.jallcom.2015.02.093

[25] Payne WH, Tennery VJ (1965) Dielectric and structural investigations of system $BaTiO_3$–$BaHfO_3$. J Am Ceram Soc 48(8):413–417. https://doi.org/10.1111/j.1151-2916.1965.tb14779.x

[26] Dobal PS, Dixit A, Katiyar RS, Yu Z, Guo R, Bhalla AS (2001) Micro-Raman scattering and dielectric investigations of phase transition behavior in the $BaTiO_3$–$BaZrO_3$ system. J Appl Phys 89(12):8085–8091. https://doi.org/10.1063/1.1369399

[27] Verbitskaia TN, Zhdanov GS, Venevtsev IN, Soloviev SP (1958) Electrical and X-ray diffraction studies of the $BaTiO_3$–$BaZrO_3$ system. Sov Phys Crystallogr 3:182–192

[28] Kalyani AK, Brajesh K, Senyshyn A, Ranjan R (2014) Orthorhombic-tetragonal phase coexistence and enhanced piezo-response at room temperature in Zr, Sn, and Hf modified $BaTiO_3$. Appl Phys Lett 104(25):252906. https://doi.org/10.1063/1.4885516

[29] Avrahami Y, Tuller HL (2004) Improved electromechanical response in rhombohedral $BaTiO_3$. J Electroceram 13(1–3):463–469. https://doi.org/10.1007/s10832-004-5143-6

[30] Zhou C, Liu WF, Xue DZ, Ren XB, Bao HX, Gao JH, Zhang LX (2012) Triple-point-type morphotropic phase boundary based large piezoelectric Pb-free material-Ba$(Ti_{0.8}Hf_{0.2})O_3$–$(Ba_{0.7}Ca_{0.3})TiO_3$. Appl Phys Lett 100(22):222910. https://doi.org/10.1063/1.4724216

[31] Wang DL, Jiang ZH, Yang B, Zhang ST, Zhang MF, Guo FF, Cao WW (2014) Phase transition behavior and high piezoelectric properties in lead-free $BaTiO_3$–$CaTiO_3$–$BaHfO_3$ ceramics. J Mater Sci 49(1):62–69. https://doi.org/10.1007/s10853-013-7650-9

[32] Wang DL, Jiang Z, Yang B, Zhang ST, Zhang MF, Guo FF, Cao WW (2014) Phase diagram and enhanced piezoelectric response of lead-free $BaTiO_3$–$CaTiO_3$–$BaHfO_3$ system. J Am Ceram Soc 97(10):3244–3251. https://doi.org/10.1111/jace.13137

[33] Zhao CL, Wu WJ, Wang H, Wu JA (2016) Site engineering and polarization characteristics in $(Ba_{1-y}Ca_y)(Ti_{1-x}Hf_x)O_3$ lead-free ceramics. J Appl Phys 119(2):24108. https://doi.org/10.1063/1.4939762

[34] Zhao CL, Feng YM, Wu HP, Wu JG (2016) Phase boundary design and high piezoelectric activity in (1 − x)$(Ba_{0.93-}Ca_{0.07})TiO_3$–x$Ba(Sn_{1-y}Hf_y)O_3$ lead-free ceramics. J Alloys Compd 666:372–379. https://doi.org/10.1016/j.jallcom.2016.01.105

[35] Zhao CL, Wang H, Xiong J, Wu JG (2016) Composition-driven phase boundary and electrical properties in $(Ba_{0.94-}Ca_{0.06})(Ti_{1-x}M_x)O_3$ (M = Sn, Hf, Zr) lead-free ceramics. Dalton Trans 45(15):6466–6480. https://doi.org/10.1039/c5dt04891e

[36] Di Loreto A, Machado R, Frattini A, Stachiotti MG (2017) Improvement in the sintering process of $Ba_{0.85}Ca_{0.15}Zr_{0.1}T$

$i_{0.9}O_3$ ceramics by the replacement of Zr by Hf. J Mater Sci: Mater Electron 28(1):588–594. https://doi.org/10.1007/s10854-016-5562-6

[37] Yang Y, Zhou Y, Ren J, Zheng QJ, Lam KH, Lin DM (2018) Coexistence of three ferroelectric phases and enhanced piezoelectric properties in $BaTiO_3$–$CaHfO_3$ lead-free ceramics. J Eur Ceram Soc 38(2):557–566. https://doi.org/10.1016/j.jeurceramsoc.2017.09.023

[38] Tian HY, Wang Y, Miao J, Chan HLW, Choy CL (2007) Preparation and characterization of hafnium doped barium titanate ceramics. J Alloys Compd 431(1–2):197–202. https://doi.org/10.1016/j.jallcom.2006.05.037

[39] Wang JC, Zheng P, Yin RQ, Zheng LM, Du J, Zheng L, Deng JX, Song KX, Qin HB (2015) Different piezoelectric grain size effects in $BaTiO_3$ ceramics. Ceram Int 41(10):14165–14171. https://doi.org/10.1016/j.ceramint.2015.07.039

[40] Zhi Y, Chen A, Guo RY, Bhalla AS (2002) Piezoelectric and strain properties of $Ba(Ti_{1-x}Zr_x)O_3$ ceramics. J Appl Phys 92(3):1489–1493. https://doi.org/10.1063/1.1487435

[41] Li W, Xu ZJ, Chu RQ, Fu P, Zang GZ (2010) Dielectric and piezoelectric properties of $Ba(Zr_xTi_{1-x})O_3$ lead-free ceramics. Braz J Phys 40(3):353–356. https://doi.org/10.1590/S0103-97332010000300018

[42] Yao YG, Zhou C, Lv DC, Wang D, Wu HJ, Yang YD (2012) Large piezoelectricity and dielectric permittivity in $BaTiO_3$–$xBaSnO_3$ system: the role of phase coexisting. EPL (Europhys Lett) 98(2):27008. https://doi.org/10.1209/0295-5075/98/27008

[43] Karaki T, Yan K, Adachi M (2007) Barium titanate piezoelectric ceramics manufactured by two-step sintering. Jpn J Appl Phys 46(10B):7035–7038. https://doi.org/10.1143/jjap.46.7035

[44] Tsurumi T, Li J, Hoshina T, Kakemoto H, Nakada M, Akedo J (2007) Ultrawide range dielectric spectroscopy of $BaTiO_3$-based perovskite dielectrics. Appl Phys Lett 91(18):182905. https://doi.org/10.1063/1.2804570

[45] Hoshina T, Takizawa K, Li J, Kasama T, Kakemoto H, Tsurumi T (2008) Domain size effect on dielectric properties of barium titanate ceramics. Jpn J Appl Phys 47(9):7607–7611. https://doi.org/10.1143/jjap.47.7607

[46] Jaffe B, Cook WR, Jafie H (1971) Piezoelectric ceramics. Academic Press, London

[47] Devonshire AF (1949) XCVI. Theory of barium titanate-part 1. Philos Mag 40(309):1040–1063. https://doi.org/10.1080/14786444908561372

[48] Tian HY, Wang Y, Miao J, Chan HLW, Choy CL (2007) Preparation and characterization of hafnium doped barium titanate ceramics. J Alloys Compd 431(1–2):197–202. https://doi.org/10.1016/j.jallcom.2006.05.037

[49] Anwar S, Sagdeo PR, Lalla NP (2006) Crossover from classical to relaxor ferroelectrics in $BaTi_{1-x}Hf_xO_3$ ceramics. J Phys: Condens Matter 18(13):3455–3468. https://doi.org/10.1088/0953-8984/18/13/013

[50] Zhou C, Ren XB, Tan XL, Guo HZ (2014) Unique single-domain state in a polycrystalline ferroelectric ceramic. Phys Rev B 89(10):100104. https://doi.org/10.1103/PhysRevB.89.100104

[51] Mitoseriu L, Tura V, Papusoi C, Osaka T, Okuyama M (1999) A comparative study of the grain size effects on ferro-para phase transition in barium titanate ceramics. Ferroelectrics 223(1):99–106. https://doi.org/10.1080/00150199908260558

[52] Kuwabara M, Matsuda H, Kurata N, Matsuyama E (1997) Shift of the curie point of barium titanate ceramics with sintering temperature. J Am Ceram Soc 80(10):2590–2596. https://doi.org/10.1111/j.1151-2916.1997.tb03161.x

[53] Li BR, Wang XH, Li LT, Zhou H, Liu XT, Han XQ, Zhang YC, Qi XW, Deng XY (2004) Dielectric properties of fine-grained $BaTiO_3$ prepared by spark-plasma-sintering. Mater Chem Phys 83(1):23–28. https://doi.org/10.1016/j.matchemphys.2003.08.009

[54] Arlt G, Hennings D, de With G (1985) Dielectric properties of fine-grained barium titanate ceramics. J Appl Phys 58(4):1619–1625. https://doi.org/10.1063/1.336051

[55] Mitoseriu L, Tura V, Papusoi C, Osaka T, Okuyama M (1999) A comparative study of the grain size effects on ferro-para phase transition in barium titanate ceramics. Ferroelectrics 223(1):99–106. https://doi.org/10.1080/00150199908260558

[56] Zhu LF, Zhang BP, Zhao L, Li S, Zhou Y, Shi XC, Wang N (2016) Large piezoelectric effect of $(Ba,Ca)TiO_3$–$xBa(Sn,Ti)O_3$ lead-free ceramics. J Eur Ceram Soc 36(4):1017–1024. https://doi.org/10.1016/j.jeurceramsoc.2015.11.039

[57] Zhao L, Zhang BP, Wang N, Chen JY (2017) High piezoelectricity in CuO-modified $Ba(Ti_{0.90}Sn_{0.10})O_3$ lead-free ceramics with modulated phase structure. J Eur Ceram Soc 37(4):1411–1419. https://doi.org/10.1016/j.jeurceramsoc.2016.11.028